

# Partially-coherent spirally-polarized gradual-edge imaging

Marcos Pérez-Aviño<sup>a</sup>, Rosario Martínez-Herrero<sup>b</sup>, Santiago Vallmitjana<sup>a</sup>,  
Pedro Latorre-Carmona<sup>c</sup>, Ignasi Juvells<sup>a</sup>, Artur Carnicer <sup>\*,a</sup>

*\* Corresponding author E-mail: artur.carnicer@ub.edu*

<sup>a</sup>*Universitat de Barcelona (UB), Facultat de Física, Departament de Física Aplicada, Martí i Franquès 1, 08028 Barcelona, Spain*

<sup>b</sup>*Universidad Complutense de Madrid, Facultad de Ciencias Físicas, Departamento de Óptica, Ciudad Universitaria, 28040 Madrid, Spain*

<sup>c</sup>*Universitat Jaume I, Institute of New Imaging Technologies, Campus Riu Sec, 12071 Castelló de la Plana, Spain*

---

## Abstract

In this work we develop a partially-coherent spirally-polarized imaging system for generating gradual edge detection images. A rotating diffuser is used for producing illumination sources with tunable degree of coherence. Using a 4f configuration, the frequency content of the image is modified by means of a vortex half-wave retarder as a spatial filter. Accordingly, we analytically describe a spirally-polarized imaging system illuminated with a Gauss-Schell source using paraxial coherence-polarization theory. Numerical simulations and experimental results demonstrate the validity of our approach. We use a referenceless spatial content descriptor to assess the quality of the recorded images as a function of the coherence state of the source.

*Keywords:* Fourier optics, Spatial filtering, Coherence, Polarization

---

## 1. Introduction

The theory that describes the statistical properties of electromagnetic fields allows for a precise characterization of coherent phenomena [1–3]. This framework was extended to jointly describe coherence and polarization using a unified vector formalism [4–6]. Moreover, a generalization to partially coherent focused beams was introduced in [7, 8]. On the other hand, the development of partially coherent sources with tunable degree of coherence is a topic of remarkable interest when dealing with experimental setups [9–13]. Very recently, some authors have proposed spatial filtering systems for producing beams with a given degree of coherence [14, 15].

Vortex half-wave retarders (VHR) are useful for producing light beams with radial, azimuthal or spiral polarization and also as a way of enhancing the edges of the image [16, 17]. Similar results are also obtained by means of spiral phase

plates, as in [18]. In the present work we demonstrate the feasibility of producing  
 15 tunable gradual edge detection on the recorded image by means of a partially-  
 coherent spirally-polarized 4f imaging system. Interestingly, we found that the  
 partial edge enhancement effect results in an improvement of the spatial quality  
 content of the processed images. To the best of our knowledge, this is the first  
 time this approach is described.

20 The paper is organized as follows: in section 2, we mathematically describe  
 a 4f processing system with a VHR filter placed at the Fourier plane and illumi-  
 nated with a Gauss-Schell model source. Then, we present an experiment that  
 demonstrates the results predicted by our theoretical approach. In section 4, we  
 discuss the behavior of the recorded images by means of the analysis of the image  
 25 histograms and the use of the Blind/Referenceless Image Quality Evaluator  
 (BRISQUE) [19]. The use of this descriptor is very appropriate because it does  
 not require any perfect reference to assess the quality of the image. Finally, we  
 present our conclusions.

## 2. Mathematical description of a partially coherent, radially polar- 30 ized 4f imaging system

Figure 1 depicts a 4f optical system and the variables used in the present  
 analysis. The object  $g(x_0, y_0)$  is placed at the front focal plane of lens  $L_1$  and  
 illuminated with a totally polarized beam  $u(x_0, y_0)\vec{E}_0$ . Beam  $\vec{E}_0$  is linearly po-  
 larized i.e.  $\vec{E}_0 = (\cos \beta, \sin \beta)$ . Coordinate systems  $(x_0, y_0)$ ,  $(x', y')$  and  $(x, y)$   
 35 refer to the input, Fourier and output planes, respectively. Polar coordinates  
 $(r', \varphi')$  (Fourier plane) and  $(r, \varphi)$  (output plane) are also used. In what fol-  
 lows,  $u(x_0, y_0)$  is assumed to be a stochastic process, being  $\Gamma(x_1, y_1, x_2, y_2) =$   
 $\langle u^*(x_1, y_1)u(x_2, y_2) \rangle$  the mutual coherence function.

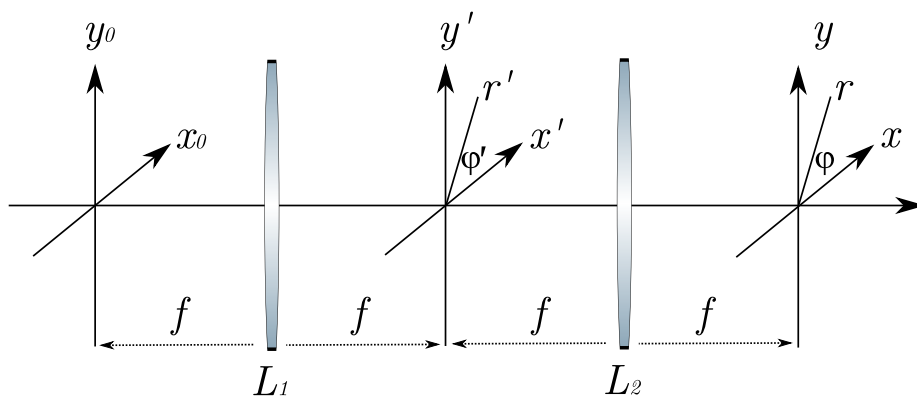


Figure 1: 4f setup

A VHR filter  $\hat{M}$  is set at the back focal plane of  $L_1$  (Fourier plane). The Jones matrix of such a device is described by

$$\hat{M} = \begin{pmatrix} \cos \varphi' & \sin \varphi' \\ -\sin \varphi' & \cos \varphi' \end{pmatrix}. \quad (1)$$

The optical system is described by using paraxial propagation theory [20] and accordingly, the electric field at the back focal plane of tube lens  $L_2$  (output plane) reads:

$$\vec{E}(x, y) \propto \iint g(\bar{x} - x, \bar{y} - y) u(\bar{x} - x, \bar{y} - y) \vec{E}_0 \hat{N}(\bar{x}, \bar{y}) d\bar{x} d\bar{y} \quad (2)$$

where matrix  $\hat{N}$  is the optical Fourier transform of  $\hat{M}$ , i.e.:

$$\hat{N}(r, \varphi) = \int \hat{M}(r', \varphi') \exp\left(i \frac{2\pi}{\lambda f} (r' r \cos(\varphi' - \varphi))\right) r' dr' d\varphi'. \quad (3)$$

Using the previous equation, it is straightforward to demonstrate that matrix  $\hat{N}$  reads

$$\hat{N}(r, \varphi) = 2\pi i \begin{pmatrix} \cos \varphi & \sin \varphi \\ -\sin \varphi & \cos \varphi \end{pmatrix} \int_0^R J_1\left(\frac{2\pi r' r}{\lambda f}\right) r' dr', \quad (4)$$

where  $R$  is the radius of filter  $\hat{M}$  and  $J_1(x)$  is the Bessel function of the first kind and order 1. Interestingly, depending on the polarization direction of the input beam  $\vec{E}_0 = (\cos \beta, \sin \beta)$ , the electric field at the back focal plane  $\vec{E}(x, y)$  is spirally polarized. Then, the recorded intensity  $I(x, y)$  is described by

$$I(x, y) \propto \int g(x_1 - x, y_1 - y) g(x_2 - x, y_2 - y) \Gamma(x_1 - x, y_1 - y, x_2 - x, y_2 - y) \text{Tr} \left[ \hat{N}^\dagger(x_1, y_1) \vec{E}_0^\dagger \vec{E}_0 \hat{N}(x_2, y_2) \right] dx_1 dy_1 dx_2 dy_2. \quad (5)$$

Symbol  $\dagger$  and operator  $\text{Tr}[\ ]$  stand for conjugate transpose matrix and matrix trace respectively;  $x_1, y_1, x_2$  and  $y_2$  are dummy variables. In particular, for linearly polarized input beams  $\vec{E}_0 = (\cos \beta, \sin \beta)$  the trace term reads:

$$\begin{aligned} \text{Tr} \left[ \hat{N}^\dagger(x_1, y_1) \vec{E}_0^\dagger \vec{E}_0 \hat{N}(x_2, y_2) \right] &= 4\pi^2 \cos(\varphi_1 - \varphi_2) \int_0^R J_1\left(\frac{2\pi r' r_1}{\lambda f}\right) r' dr' \\ &\times \int_0^R J_1\left(\frac{2\pi r' r_2}{\lambda f}\right) r' dr', \end{aligned} \quad (6)$$

where  $\varphi_1$  and  $\varphi_2$  are the dummy angular coordinates related to  $x_1, y_1$  and  $x_2$  and  $y_2$ , respectively. For a partially coherent source that fulfills the Gauss-Schell model [2], the mutual coherence function  $\Gamma(\ )$  reads

$$\Gamma(x_1, y_1, x_2, y_2) = C \exp\left(-\frac{x_1^2 + x_2^2 + y_1^2 + y_2^2}{4\sigma^2}\right) \exp\left(-\frac{(x_1 - x_2)^2 + (y_1 - y_2)^2}{2\mu^2}\right), \quad (7)$$

where  $C$  is a constant and  $\sigma$  and  $\mu$  describe the spatial width of the source and the longitude of coherence, respectively. In particular, special cases  $\mu/\sigma \rightarrow 0$  and  $\mu/\sigma \rightarrow \infty$  describe totally incoherent and totally coherent sources respectively. For an incoherent source, the mutual coherence function fulfills  $\Gamma(x_1, y_1, x_2, y_2) = \delta(x_1 - x_2)\delta(y_1 - y_2)$  and thus, the intensity  $I(x, y)$  becomes

$$I(x, y) = \int g(x_1 - x, y_1 - y)^* g(x_1 - x, y_1 - y) \text{Tr} \left[ \hat{N}^\dagger(x_1, y_1) \vec{E}_0^\dagger \vec{E}_0 \hat{N}(x_1, y_1) \right] dx_1 dy_1 = \int |g(x_1 - x, y_1 - y)|^2 \text{Tr} \left[ \hat{N}^\dagger(x_1, y_1) \vec{E}_0^\dagger \vec{E}_0 \hat{N}(x_1, y_1) \right] dx_1 dy_1. \quad (8)$$

Note that  $h_i(x, y) = \text{Tr} \left[ \hat{N}^\dagger(x, y) \vec{E}_0^\dagger \vec{E}_0 \hat{N}(x, y) \right]$  is the incoherent point spread function of the system.

For a full coherent source, the mutual coherence function is simply  $\Gamma(x_1, y_1, x_2, y_2) = u^*(x_1, y_1)u(x_2, y_2)$  and consequently, the intensity reads

$$I(x, y) \propto \int g^*(x_1 - x, y_1 - y) u^*(x_1, y_1) g(x_2 - x, y_2 - y) u(x_2, y_2) \text{Tr} \left[ \hat{N}^\dagger(x_1, y_1) \vec{E}_0^\dagger \vec{E}_0 \hat{N}(x_2, y_2) \right] dx_1 dy_1 dx_2 dy_2 = \left| \int g^*(\bar{x} - x, \bar{y} - y) u^*(\bar{x}, \bar{y}) \vec{E}_0 \hat{N}(\bar{x}, \bar{y}) d\bar{x} d\bar{y} \right|^2. \quad (9)$$

In order to provide more insight into the behavior of the described system, we calculated the intensity  $I(x, y)$  using Eq. (5) for different values of parameter  $\mu$  (Eq. (7)); the intensity over the test object is nearly constant. The test object  $g(x, y)$  is a 201x201 pixels image shown in Fig. 2(a); the length of the image width is set to 20 mm (the radius of the star is 10 mm) and  $\vec{E}_0$  is linearly polarized. Figures 2(b-f) display the resulting distributions  $I(x, y)$  for  $\mu = 10^6$ , 100, 10, 3 and 0.1 mm respectively.

Figure 2(b) shows the resulting image for  $\mu = 10^6$ ; the VHR filter produces an edge enhancement effect, removing all light but from the edges. Moreover, the fine details at the center of the star are lost due to the coherent cut-off frequency. Figures 2(c-d) were calculated using  $\mu = 100$  and  $\mu = 10$  respectively; note that Figs. 2(b-d) are almost indistinguishable. On the other hand, Fig. 2(f) displays the most incoherent case considered in this set of simulations ( $\mu = 0.1$  mm). As expected, the coherent cut-off frequency limit is over-passed at the expense of a contrast inversion effect [20]; moreover, no edge enhancement is reported. Finally, Fig. 2(e) ( $\mu = 3$  mm) shows an intermediate state: edge enhancement is present, but some light is detectable in the pixels that do not belong to the edges of the original image. According to these results, it would be possible to produce gradual edge-enhancement images by tuning the coherence of the source. Interestingly, changes in the behavior of the final image are only noticeable for  $\mu$  values small enough so that the illumination source can be considered nearly incoherent.

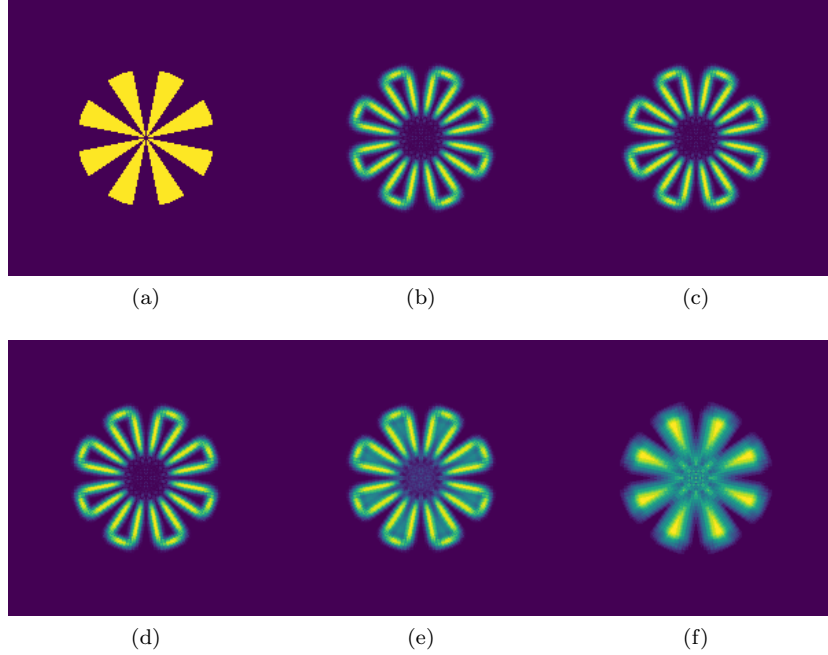


Figure 2: Image formation simulations using partially coherent light. Images are presented in false color using the viridis colormap: (a) test object; (b)  $I(x, y)$  with  $\mu = 10^6$  mm; (c)  $I(x, y)$  with  $\mu = 100$  mm; (d)  $I(x, y)$  with  $\mu = 10$  mm; (e)  $I(x, y)$  with  $\mu = 3$  mm; (f)  $I(x, y)$  with  $\mu = 0.1$  mm..

### 3. Experimental set-up

In order to test the theoretical approach described above, an optical exper-  
65 iment has been conducted. Figure 3 shows a sketch of the optical setup and a  
picture of the system. The sample  $g(x, y)$  is imaged by means of a bench mi-  
croscope comprised of a NA=0.45 microscope lens (ML), a tube lens (TL) and  
a CCD camera. Object  $g(x, y)$  and a VHR filter (Thorlabs WPV10L-633) are  
set at the front and back focal planes of the objective lens respectively. Since  
70  $f_{ML} \neq f_{TL}$ , coordinates  $(x, y)$  at the CCD plane have to be scaled according to  
a magnification factor  $M = -\frac{f_{TL}}{f_{ML}}$ . The sample is illuminated by means of a  
condenser system able to tune the degree of coherence of the beam.

A He-Ne laser ( $\lambda=632.8$  nm) connected to an optical fiber produces a diverg-  
ing wave located at point  $S$ . The beam is propagated through lenses  $L_A$ ,  $L_B$   
75 and  $L_C$ ;  $S'$  and  $S''$  are intermediate images of the point source  $S$  after lenses  $L_A$   
and  $L_C$  respectively. A rotating diffuser is placed between lenses  $L_A$  and  $L_B$ ;  
the position of the diffuser can be modified in order to change the coherence of  
the light that illuminates the sample, being  $d$  the distance between  $S'$  and the  
difusser. As we show below,  $d$  is a handy parameter to characterize the degree

80 of coherence of the beam.

The coherence length  $\mu$  at the sample plane has been theoretically estimated using the VanCitter-Zernike theorem, and taking into account the specifications of the condenser system. As shown in [21] and in [5] (pages 31 and 32), in an experimental setup used for producing a Gauss-Schell source, parameters  $\sigma$  and  $\mu$  are related by means of the following equation

$$\mu = \frac{D\lambda}{\sqrt{2\pi}\sigma}, \quad (10)$$

where  $D$  is the distance between the rotating diffuser and the sample.

We evaluated the effective coherence length on the sample  $\mu'(d)$  for the present optical setup. First, the positions  $D'(d)$  of the image of the difusser through lenses  $L_B$  and  $L_C$  were calculated. Second, rough estimations of the beam widths  $\sigma(d)$  at the difusser plane were obtained; then, effective widths on the sample  $\sigma'(d)$  were determined by considering the magnification through the optical system. Finally,  $\mu'(d)$  was assessed by using the effective parameters  $D'(d)$  and  $\sigma'(d)$  on Eq. 10. Finally, we estimated that  $\mu$  values varies from 0.14 to 0.0038 mm for  $0.7 \leq d \leq 25mm$ . The specifications of the optical system are summarized in Table 1.

90

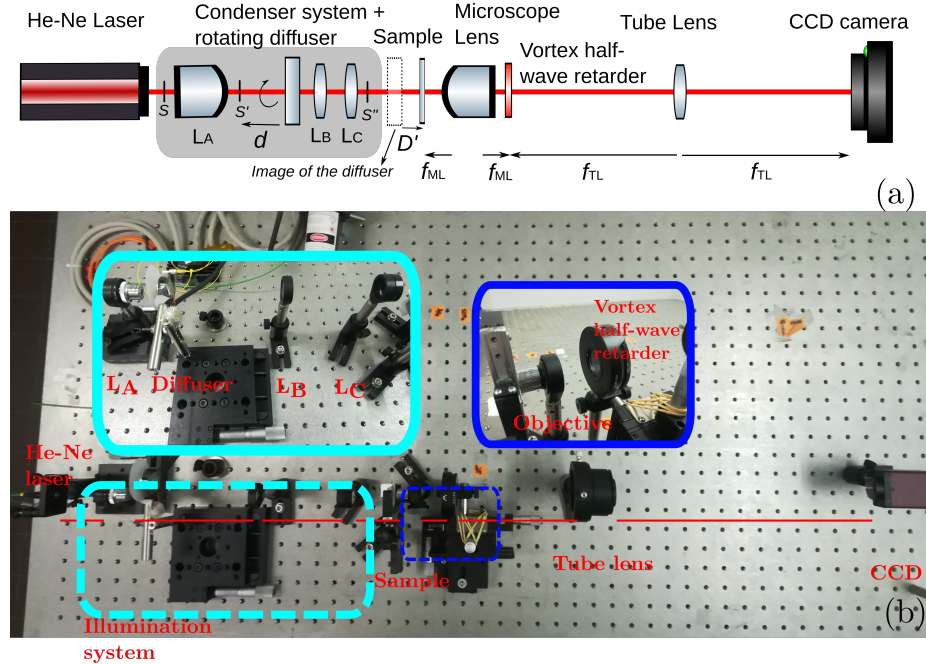


Figure 3: (a) Sketch of the optical setup; (b) experimental optical arrangement

Lens $L_A$	$f_A = 13$ mm, NA=0.45
Lens $L_B$	$f_B = 150$ mm
Lens $L_C$	$f_C = 25$ mm
Microscope Lens (ML)	$f_{ML} = 16$ mm, NA=0.45
Tube Lens (TL)	$f_{TL} = 200$ mm
Distance $L_A - S'$	$\approx 25$ mm
Distance $L_A - L_B$	170 mm
Distance $L_B - L_C$	115 mm
Distance $L_C - \text{Sample}$	54 mm
Range distance $d$	0.7 - 25.5 mm
Source wavelength	632.8 nm
Object area	0.64 x 0.44 mm
# pixels	1280 x 960
Bit depth	8

Table 1: Specifications of the optical system.

#### 4. Results

Three objects have been used: a USAF-1951 frequency test and two different pictures of diatoms. These images have been processed with and without the VHR filter. For each of the six cases considered, twenty different intensity images have been recorded at different distances  $d$ . Four images of each set  
95 recorded at  $d = 0.7, 5.23, 13.8$  and  $25.5$  mm are shown in Fig. 4 ( $\mu = 0.14, 0.018, 0.007, 0.0038$  mm respectively). The images in rows 1, 3 and 5 were obtained without the VHR filter; images displayed in rows 2, 4 and 6 were acquired using the VHR filter.

100 In the images of the first column, high coherence noise is noticeable and in those where the polarizing filter is present a clear edge enhancement effect is detected. The second and third columns show a reduction of the coherent noise; when the VHR filter is used the background intensity increases. In the last column, all coherent effects, including edge enhancement, disappear. The final  
105 images, with and without the filter, are very similar.

An interesting behavior is found when analyzing the histograms of the images [Fig. 5]. Note that when the filter is used the histograms are shifted towards lower pixel values as the coherence of the light increases. This is consistent with Fig. 4: whereas filtered images illuminated with partially coherent light contain  
110 almost only black pixels, almost incoherent light produces images with a more energetic background.

Although informative, histograms do not provide any clue about the quality of the processed images. In the present work, we are interested in the assessment of the quality of the recorded images, since we are aiming at determining  
115 under which conditions we get the best results. One of the most accepted blind image quality estimators is BRISQUE. This approach is chosen because there is no reference image among the recorded ones whose quality can be considered as perfect. This method builds local spatial features for images (images

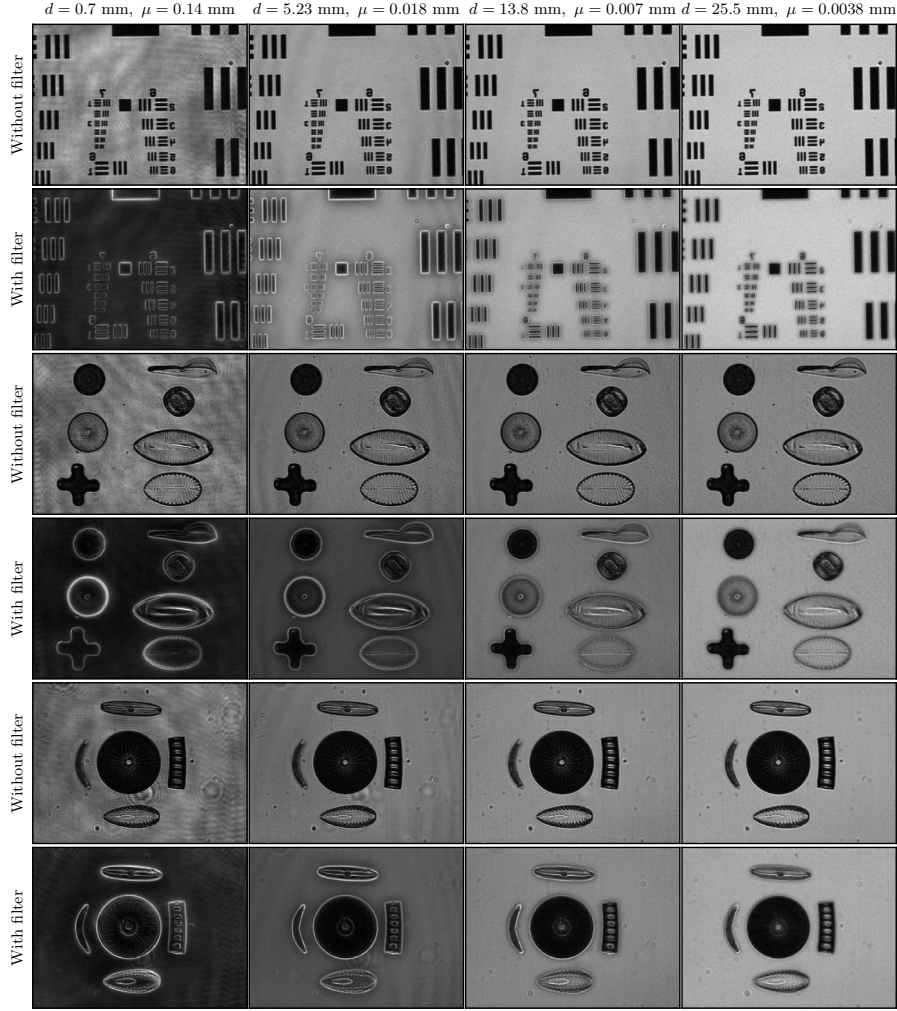


Figure 4: Recorded images  $I(x, y)$  at different distances  $d$  with their corresponding coherence length  $\mu$ . The results shown in the first, third and fifth rows do not use the VHR filter. The second, fourth and, sixth rows correspond to the images recorded with the filter.

120 patches of size typically  $7 \times 7$ ) called subtracted contrast normalized coefficients and hypothesize on the fact that these coefficients have characteristic  
 statistical properties that are changed under the presence of a distortion. In particular, authors in [19] model these coefficients when no distortion appears  
 as asymmetric generalized Gaussian distributions [22]. Finally, a mapping is learned from feature space formed by the coefficients of the asymmetric  
 125 generalized Gaussian distributions and the quality scores for the LIVE Image Quality Assessment Database [23], using a support vector machine regression [24]. In

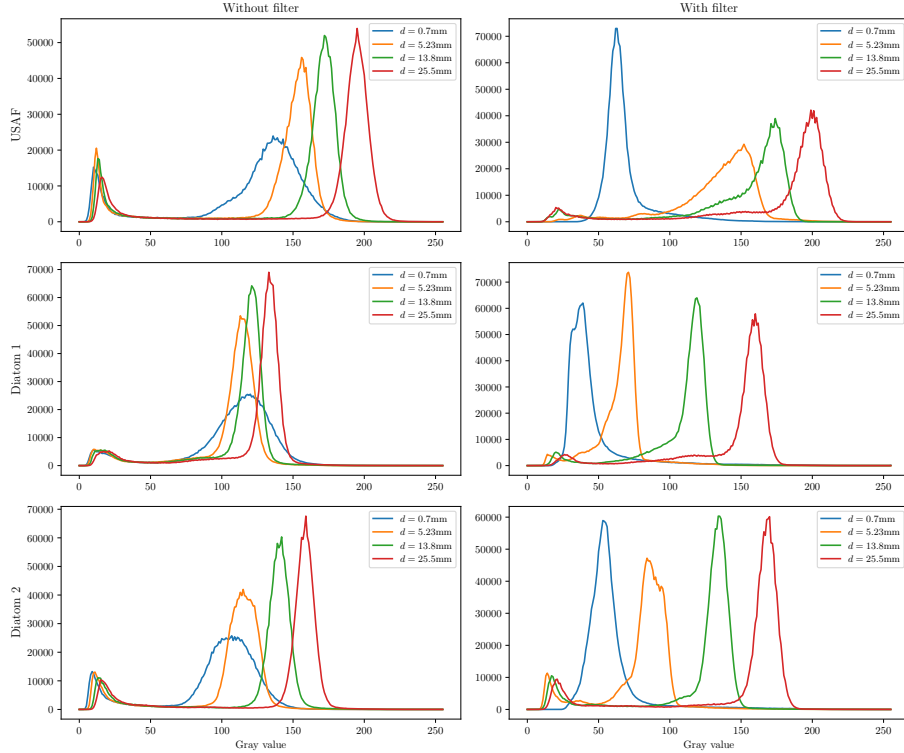


Figure 5: Histograms of the recorded images. The first column corresponds to images with the VHR filter and the second, without. USAF-1951 test target, the first and second diatom sets are represented in rows 1, 2, and 3, respectively.

the implementation we used, available at [https://github.com/gregfreeman/image\\_quality\\_toolbox](https://github.com/gregfreeman/image_quality_toolbox), this quality index varies between 0 and 100 being 0 an indicator of a perfect quality .

130 The BRISQUE scores of each set of images are shown in Fig. 6. The same trend for all the cases considered is detected: images recorded using the VHR filter produce (i) better BRISQUE scores for small values of  $d$  (more coherent cases) and (ii) a minimum BRISQUE value is always detected.

## 5. Concluding remarks

135 In the present paper we found that the combined use of a partially coherent light source and a vortex half-wave retarder makes possible designing imaging systems able to produce gradual edge enhanced images. In the experiments, we used a conventional 4f imaging system with coherent-tunable illumination and a vortex half-wave retarder placed at the Fourier plane. In this way, the  
 140 final image is spirally polarized. The combination of coherence and polarization

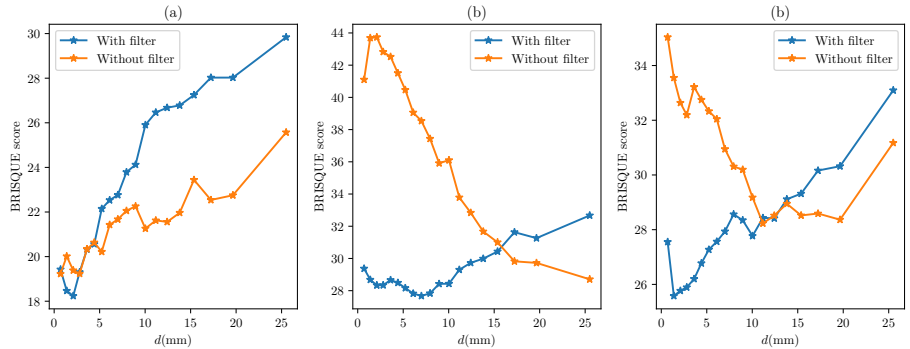


Figure 6: BRISQUE scores for each set of images. (a) USAF-1951 frequency test; (b) and (c) the two sets of diatoms. Recall that lower values represent better image quality.

effects results in a gradual edge detection and in a modification of the spatial quality content of the final image.

We assessed the quality of each image by means of the BRISQUE blind image quality estimator. We found that a minimum value of this parameter is found when using the VHR filter for a particular partially coherent state. In other words, according to BRISQUE these images present better spatial quality

**Acknowledgments**

RMH and AC acknowledges support from MINECO project number FIS2016-75147-C3-1-P.

**References**

- [1] H. Hopkins, On the diffraction theory of optical images, Proc. Math. Phys. Eng. Sci. 217 (1130) (1953) 408–432.
- [2] L. Mandel, E. Wolf, Optical coherence and quantum optics, Cambridge university press, 1995.
- [3] J. W. Goodman, Statistical optics, John Wiley & Sons, 2015.
- [4] E. Wolf, Introduction to the Theory of Coherence and Polarization of Light, Cambridge University Press, 2007.
- [5] R. Martínez-Herrero, P. M. Mejías, G. Piquero, Characterization of partially polarized light fields, Vol. 147, Springer Science & Business Media, 2009.
- [6] A. T. Friberg, T. Setälä, Electromagnetic theory of optical coherence, J. Opt. Soc. Am. A 33 (12) (2016) 2431–2442.

- [7] W. Wang, A. T. Friberg, E. Wolf, Focusing of partially coherent light in systems of large fresnel numbers, *J. Opt. Soc. Am. A* 14 (2) (1997) 491–496. 165
- [8] M. R. Foreman, P. Török, Focusing of spatially inhomogeneous partially coherent, partially polarized electromagnetic fields, *J. Opt. Soc. Am. A* 26 (11) (2009) 2470–2479.
- [9] P. De Santis, F. Gori, G. Guattari, C. Palma, Synthesis of partially coherent fields, *J. Opt. Soc. Am. A* 3 (8) (1986) 1258–1262. 170
- [10] G. Indebetouw, Synthesis of polychromatic light sources with arbitrary degrees of coherence: some experiments, *J. Mod. Opt.* 36 (2) (1989) 251–259.
- [11] D. Mendlovic, G. Shabtay, A. W. Lohmann, Synthesis of spatial coherence, *Opt. Lett.* 24 (6) (1999) 361–363. 175
- [12] M. Santarsiero, R. Martínez-Herrero, D. Maluenda, J. De Sande, G. Piquero, F. Gori, Partially coherent sources with circular coherence, *Opt. Lett.* 42 (8) (2017) 1512–1515.
- [13] Y. Cai, Y. Chen, J. Yu, X. Liu, L. Liu, Generation of partially coherent beams, *Prog. Optics* 62 (2017) 157–223. 180
- [14] T. D. Visser, G. P. Agrawal, P. W. Milonni, Fourier processing with partially coherent fields, *Opt. Lett.* 42 (2017) 4600–4602.
- [15] T. Wu, C. Liang, F. Wang, Y. Cai, Shaping the intensity and degree of coherence of a partially coherent beam by a 4 f optical system with an amplitude filter, *J. Opt.* 19 (12) (2017) 124010. 185
- [16] B. Zhang, Z. Chen, H. Sun, J. Xia, J. Ding, Vectorial optical vortex filtering for edge enhancement, *J. Opt.* 18 (3) (2016) 035703.
- [17] B. B. Ram, P. Senthilkumaran, A. Sharma, Polarization-based spatial filtering for directional and nondirectional edge enhancement using an s-waveplate, *Appl. Opt.* 56 (11) (2017) 3171–3178. 190
- [18] S. Fürhapter, A. Jesacher, S. Bernet, M. Ritsch-Marte, Spiral phase contrast imaging in microscopy, *Opt. Express* 13 (3) (2005) 689–694.
- [19] A. Mittal, A. K. Moorthy, A. C. Bovik, No-reference image quality assessment in the spatial domain, *IEEE Trans. Image Process.* 21 (12) (2012) 4695–4708. 195
- [20] J. W. Goodman, *Introduction to Fourier optics*, Roberts and Company Publishers, 2005.
- [21] P. De Santis, F. Gori, G. Guattari, C. Palma, An example of a Collett-Wolf source, *Opt. Commun.* 29 (3) (1979) 256–260.

- 200 [22] N.-E. Lasmar, Y. Stitou, Y. Berthoumieu, Multiscale skewed heavy tailed model for texture analysis, in: Image Processing (ICIP), 2009 16th IEEE International Conference on, IEEE, 2009, pp. 2281–2284.
- [23] H. R. Sheikh, M. F. Sabir, A. C. Bovik, A statistical evaluation of recent full reference image quality assessment algorithms, IEEE Trans. Image Process. 15 (11) (2006) 3440–3451.
- 205 [24] B. Schölkopf, A. J. Smola, R. C. Williamson, P. L. Bartlett, New support vector algorithms, Neural comput. 12 (5) (2000) 1207–1245.